Accurate targeting in robot-assisted TCM pulse diagnosis using adaptive sensor fusion

Jingjing Luo[1,*+], Chun Ouyang[1,* +], Xiaokai Nie[2], Wenjie Yin[3], Feng Lin[1], Hong Lu[4], Yuzhu Guo[5,+]

[1]Institute of AI and Robotics, FAET, Fudan University, P.R.China
[2]School of Mathematics, The University of Manchester, UK
[3]School of Electrical Engineering and Computer Science, KTH Royal Institute of Technology, Sweden
[4]Key Laboratory of Intelligent Information Processing, Fudan University, P.R.China
[5]School of Automation Science and Electrical Engineering, Beihang University, P.R.China

---

ABSTRACT

Accurate position targeting plays an important role in the study of human-robot interaction under dynamic environments. In particular, the accuracy of diagnose positions at wrist needs to be addressed for robot-assisted Traditional Chinese Medicine (TCM) pulse diagnosis. In this work, imaging photoplethysmography (iPPG) which measures the physiological changes of artery is used as an extra modal information in addition to computer vision at localization, to alleviate the effect of approaching distance varying during the robot arm movement. Both computer vision and iPPG are fed into a convolutional neural networks (CNN), which boosts the accuracy at targeting of TCM radial artery of wrist. Changes of their weights reflect the adaptation of the CNN to distance varying.

Keywords: Adaptive sensor fusion, multimodal deep learning, robot-assisted TCM diagnosis, accurate targeting

INTRODUCTION

Robot-assisted diagnosis has become an applied medical examination procedure,

*: Authors contribute to this work equally
+: Corresponding authors

making use of competent proprioception sensors and autonomous robotic actuators to deliver enhanced diagnostic efficiency and enriched diagnostic information [1,2]. Accurate targeting of diagnosing location is an essential element of diagnostic robot including identification of patterns of human-body parts of interest, continuously target tracking, and adaptively communicating or controlling of robot behavior during dynamic interaction. Due to the extensive applications in medical examination, there has been considerable interest in developing solutions to the accurate targeting [3,4].

Traditional Chinese Medicine (TCM) pulse diagnosis, as a key step of patient examination in oriental medicine, is usually implemented by collecting radial pulse information at structured locations of wrist, known as 'Cun' (Inch), 'Guan/Gwan' (Bar), and 'Chi' (Cubit) (Figure 1(a) and 1(b)), where the radial artery lies [5,6]. Due to TCM palpation by precise physical contact, approaching of diagnostic robot (Figure 1(c)) to the wrist becomes a critical step of robot-assisted pulse diagnosis. Autonomous targeting including position detection, tracking and robotic control is a challenge to be solved.

In this paper, a novel approach of accurate targeting of robot-assisted TCM pulse diagnosis using adaptive multimodal sensor fusion is proposed at different height. While single modality sensor cannot adapt to scene change during dynamic approaching, multimodal interfaces are applied, taking advantage of complementary information and offering multiple possibilities of sensory integration strategies. Furthermore, diagnostic robot strongly interacts with human, the clear identification of human factors is desired for better detection and can be achieved by applying physiological sensing. In this work, imaging photoplethysmography (iPPG) is used for providing cardiovascular features of examined subjects, especially the dynamic blood perfusion imaging at wrist area [7,8]. iPPG features are extracted from sequential recording of visual images equipped at the robotic hand for palpation.

For accurate targeting of TCM pulse diagnosis, an adaptive fusion approach was

applied to integrate multiple imaging sensors, which was used to guide the robot interacting and approaching the desired palpation location. A robust multimodal deep learning architecture was devised. A weighting factor was introduced to allow the adaptability capacity and scale the contribution of different modalities and the contributions from multiple modalities are valued according to the fusion hypothesis. Experiment results show that the proposed sensor fusion method offers the additional architectural flexibility to achieve the adaptive performance in palpation localization during the robotic approaching procedure.

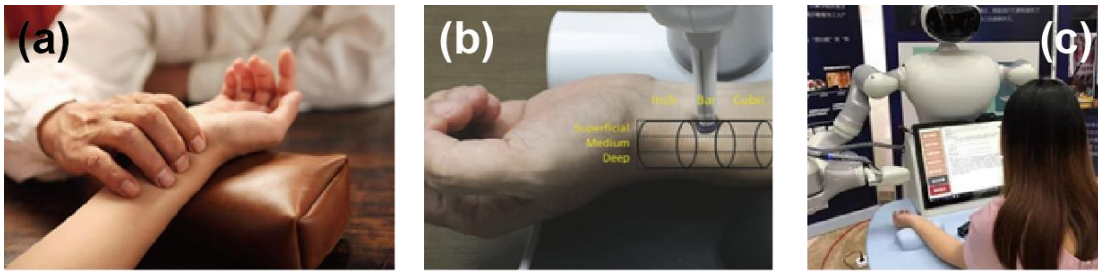

Figure 1. TCM pulse diagnosis. (a) Conventional method. (b) one type of Pulse diagnosis apparatus. (c)Robot-assisted method designed by our group.

EXPERIMENTAL SETUP

A camera was used for collecting PPG signal and wrist images of volunteers' forearm, which was placed vertically above the wrist area. The distance to wrist was controlled approximately at 5, 15, 20, 25, 30, 35 and 40cm, respectively. The resolution of each figure is 1000×1000. At each distance, for one volunteer, 20 types of hand posture were obtained, each posture were recorded for 5 seconds including 200 images. At each recording, he TCM pulse location was accessed by the experimenter and labeled using the pixel location on the recorded image sequences.

METHOD

The extraction of iPPG information uses a two-stage strategy. At the first stage, a reference PPG is extracted by using a large area mean; in the second stage, we used this reference to extract the component with similar dynamics followed by comparison for a single period time window.

Step 1: Pre-processing of PPG signal

Prior to PPG extraction, we removed the brightness of light source and the spectrum by using mean-centralization of each color signal c_t', expressed by [9]:

$$c_t = (c_t' - m_{t,M})/m_{t,M}$$

Where $m_{t,M}$ is an *M*-point running mean of color signal c_t'. We followed [9] in taking *M* corresponding to 2 s to cover at lease a single period of human heart rate.

Step 2: CHROM method for PPG extraction

Generally, "green-red difference" (G-R) method was used for PPG extraction [paper, 39], CHROM is one of commonly used G-R method, and computes PPG as a combination of color signals [14][15].

Step 3: Signal processing for PPG reference

In order to remove signal artifacts that corrupt raw PPG signals without altering the amplitude information, we combined continuous wavelet transform (CWT), local filtering using a set of adaptive Gaussian windows, and inverse CWT transform together[16][17].

Step 4: Principal component analysis (PCA) of single pixels

We applied PCA to calculate PPG signal of each pixel by combining reference PPG with RGB PPGs, where the first principal component (the largest eigenvector) was regarded as the final PPG signal at the target pixel.

Step 5: Weighted amplification of PPG signal

We computed periodical averaging of pulse cycles for both of PCA data and reference PPG to obtain one-cycle PPG signal. The weighted amplitude for each pixel was conducted by multiply of reference PPG and averaged one-cycle PPG result.

To accurately targeting at the TCM pulse location, we have worked on multiple strategies [18][19]. Firstly, a convolutional network architecture was applied, using one of the single modalities as the input, that is either the photo image of the hand or the iPPG. Images of each gesture at each distance can be lumped as samples to train an expert. Images of each iPPG result at certain distance can be lumped as samples to train a second expert.

An adaptive fusion network architecture was developed (Figure 2), by concatenating single experts at featured stages. The overall architecture is an extension of the parallel combination of each individual expert, to train adaptive fusion model in end-to-end manner. The fusion parameters adapt according to the input patterns. A proposed single expert architecture used in this work is LeNet5. At the full connection layer, projecting weights acts as the gate, mapping outputs of the experts to a probabilistically mix.

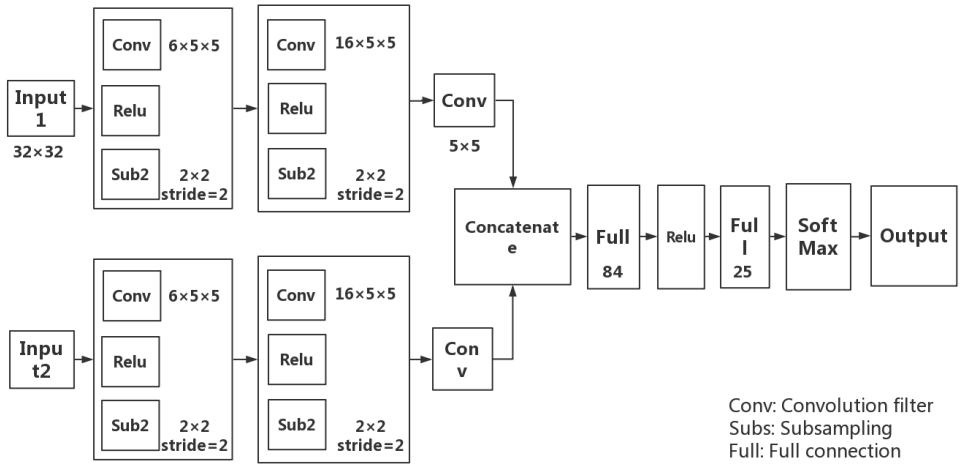

Figure 2. A proposed fusion network architecture.

EXPERIMENTAL RESULTS

The method to obtain iPPG signal was illustrated in experimental setup. Figure 3(a) shows typical imaging photoplethysmography (iPPG) signal of left hand overlapped to raw figure taken by high-resolution camera. Here, we clearly observe two significant area with high PPG intensity. which are enclosed by blue and black lines, respectively.

It is well-known that radial artery of wrist and capillary in palm localize at those positions. It is obvious that iPPG signal can be used to determine the radial artery position of wrist when the hand is lied on the desk [15]. As the intensity of iPPG signal is large enough, we could assume that iPPG signal can be used for checking radical artery pulse position even when rotation of wrist happens.

In order to confirm the assumption, more experimental study were conducted. Various gestures of hand under the camera were devised in this experiment, the results are

shown in figure 3(b-e) with slight rotation of wrist. Clear radial artery of wrist and capillary at palm can be observed in iPPG signal.

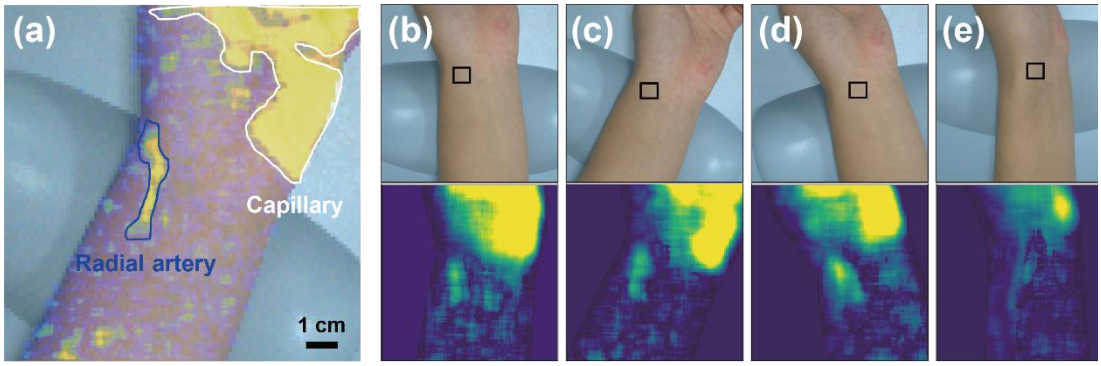

Figure 3. Typical Imaging Photoplethysmography of Left Hand.

We apply individual expert CNN models and the fusion expert CNN model, to fit for TCM pulse location at the wrist. Those labels are the pixel index of a 5×5 down sampled image in shown as figure 4(a, c, e, g). Figure 4(b, d, f, h) illustrate some samples of human forearm (the original figure on top), along with its iPPG features (the iPPG results at bottom). As expected, the fuse model out performs that of single experts (Table 1).

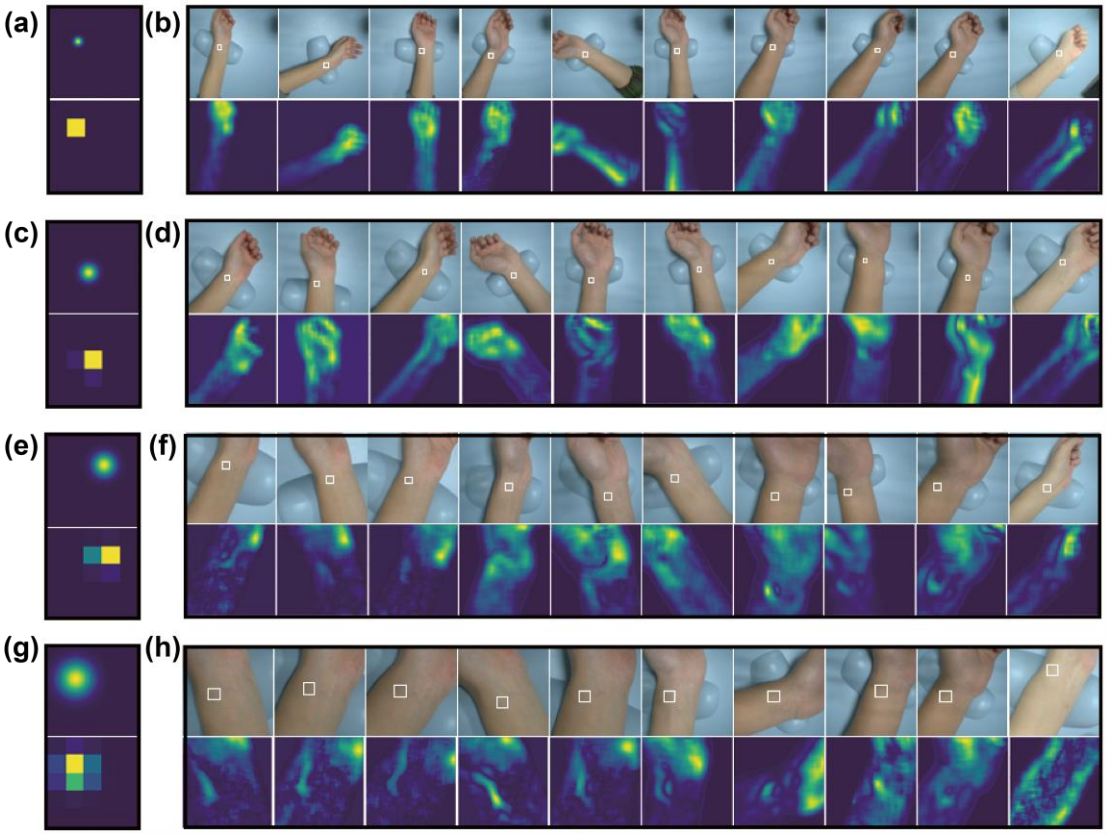

For the fuse model, we evaluate the contribution of each input modality, by calculating the coherent result of the trained model using only single input. Figure 5 shows that if the camera is at a distant location, e.g. 40cm above, then the localization fitting of original image output is more coherent to the labels thus the model is more depend on the original figure. On the other hand, if the camera is at a close distance, e.g. 5cm above the wrist, the iPPG outputs is more coherence with the labels.

Figure 4. Model predictions are consistent with experimental recordings at each distance.

Table 1. Model Comparison

Model	Estimation	Evaluation
Orig	epoch=30	Acc=83.81
iPPG	epoch=30	Acc=86.96
Fuse	epoch=30	Acc=91.55

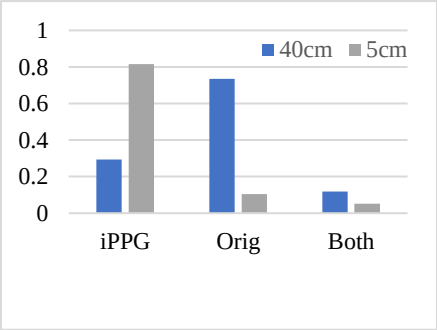

Figure 5 The coherence of fuse model outputs

CONCLUSION

In this work, we have shown iPPG which measures the physiological changes of artery is capable of indicating the location for TCM radial pulse diagnose, especially when the camera is close to the wrist. An adaptive fusion network has been developing by combined usage of static image recording as well as the iPPG images.

Experimental studies demonstrate that the proposed method can precisely locate the desired palpation position in different approaching paths by automatically adapting the weights of the two modalities. Comparison study of the performance of each modality reveals the adaptation process of the network to the distance change between the camera and the target. The proposed method provide a new pathway for the dynamical targeting and tracking of the pulse during the approach of sensor to the wrist. The integration of the new method into the TCM robot will be studied in future work.

ACKNOWLEDGEMENTS

Support from National Natural Science Foundation of China (No. 61876015) to Y. Guo. We thank Ms. Yin Tan for helping in collection of iPPG data.

REFERENCES

1. Ajoudani, A. *et al. Auton. Robots* **42,** 957–975 (2018).
2. Konstantinova, J., Jiang, A., Althoefer, K., Dasgupta, P. & Nanayakkara, T. *IEEE Sens. J.* **14,** 2490–2501 (2014).
3. Haouchine, N., Kuang, W., Cotin, S. & Yip, M. *IEEE Robot. Autom. Lett.* **3,** 2160–2165 (2018).
4. Monfaredi, R. *et al. Minim. Invasive Ther. Allied Technol.* **24,** 54–62 (2015).
5. Velik, R. *Eur. J. Integr. Med.* **7,** 321–331 (2015).
6. Ko, M. M., Lee, M. S., Birch, S. & Lee, J. A. *Eur. J. Integr. Med.* **15,** 47–63 (2017).
7. Kamshilin, A. A. *et al. Biomed. Opt. Express* **7,** 5138 (2016).
8. Corral, F., Paez, G. & Strojnik, M. *Opt. Appl.* **44,** 191–204 (2014).
9. Van Gastel, M., Stuijk, S. & De Haan, G. *IEEE Trans. Biomed. Eng.* **62,** 1425–1433 (2015).
10. Jacques, S. L. *Phys. Med. Biol.* **58,** 5007–5008 (2013).
11. Sun, Y. & Thakor, N. *IEEE Trans. Biomed. Eng.* **63,** 463–477 (2016).
12. Bousefsaf, F., Maaoui, C. & Pruski. *Biomed. Mater. Eng.* **27,** 527–538 (2016).
13. Valada, A., Vertens, J., Dhall, A. & Burgard, W. AdapNet: *Proc. - IEEE Int. Conf. Robot. Autom.* 4644–4651 (2017). doi:10.1109/ICRA.2017.7989540
14. Mees, O., Eitel, A. & Burgard, W. Choosing smartly. *IEEE Int. Conf. Intell. Robot. Syst.* **2016–Novem,** 151–156 (2016).
15. Kamshilin, A. A. *et al. Sci. Rep.* **5,** 1–9 (2015).